Bimodal Analysis Reveals a General Scaling Law Governing Nondirected and Chemotactic Cell Motility

J. Scott Gruver,[†△] Alka A. Potdar,[‡¶△] Junhwan Jeon,[‡¶] Jiqing Sai,[§] Bridget Anderson,[‖] Donna Webb,[§‖††] Ann Richmond,[§‡‡] Vito Quaranta,[§‡] Peter T. Cummings,[‡¶§§] and Chang Y. Chung[†‖*]

[†]Department of Pharmacology, [‡]Vanderbilt Integrative Cancer Biology Center, [§]Department of Cancer Biology, Vanderbilt University Medical Center, [¶]Department of Chemical and Biomolecular Engineering, and [‖]Department of Biological Sciences, Vanderbilt University, Nashville, Tennessee; [††]Vanderbilt Kennedy Center for Research on Human Development, Nashville, Tennessee; [‡‡]Department of Veterans Affairs, Nashville, Tennessee; and [§§]Center for Nanophase Materials Sciences, Oak Ridge National Laboratory, Oak Ridge, Tennessee

ABSTRACT Cell motility is a fundamental process with relevance to embryonic development, immune response, and metastasis. Cells move either spontaneously, in a nondirected fashion, or in response to chemotactic signals, in a directed fashion. Even though they are often studied separately, both forms of motility share many complex processes at the molecular and subcellular scale, e.g., orchestrated cytoskeletal rearrangements and polarization. In addition, at the cellular level both types of motility include persistent runs interspersed with reorientation pauses. Because there is a great range of variability in motility among different cell types, a key challenge in the field is to integrate these multiscale processes into a coherent framework. We analyzed the motility of *Dictyostelium* cells with bimodal analysis, a method that compares time spent in persistent versus reorientation mode. Unexpectedly, we found that reorientation time is coupled with persistent time in an inverse correlation and, surprisingly, the inverse correlation holds for both nondirected and chemotactic motility, so that the full range of *Dictyostelium* motility can be described by a single scaling relationship. Additionally, we found an identical scaling relationship for three human cell lines, indicating that the coupling of reorientation and persistence holds across species and making it possible to describe the complexity of cell motility in a surprisingly general and simple manner. With this new perspective, we analyzed the motility of *Dictyostelium* mutants, and found four in which the coupling between two modes was altered. Our results point to a fundamental underlying principle, described by a simple scaling law, unifying mechanisms of eukaryotic cell motility at several scales.

INTRODUCTION

Cell motility plays key roles in health and disease. Two forms, directed and nondirected motility, are commonly studied. Directed motility, the best-understood example of which is chemotaxis, occurs when the motility of cells is directionally biased as the result of a spatial (or possibly temporal) signal. When experimentally removed from external signals, cells remain motile, yet move in no particular direction. The two forms of motility are often studied separately and from different perspectives. Chemotaxis is often studied with the intent of elucidating the signal transduction pathways, by allowing cells to sense direction in the gradient, a process called ''directional sensing'' (1–4). Indeed, directional sensing is remarkable for its sensitivity to weak, noisy concentration gradients (5–7). Nondirected motility is often approached from the physical perspective of spontaneous ''symmetry breaking'' (8). This is because the cell must choose a direction in which to move, despite having no external signal to influence this choice. A cell with no polarity and in the absence of a directional cue is in a high symmetry state, in that all directions are equally favorable (i.e., symmetric). As the cell chooses a direction from these symmetric possibilities, the cell polarizes and begins to move in that direction, thus breaking the symmetry. Once the cell begins to move, its range of motion is restricted and therefore the cell is in a lower state of symmetry.

Despite the apparent differences between nondirected and chemotactic motility, they share many processes at the molecular, subcellular, and cellular level. Most generally, all cell movements require actin polymerization. Furthermore, signaling pathways first described to regulate directional sensing downstream of the chemoattractant receptor in *Dictyostelium* and fibroblasts were subsequently shown to be spontaneously activated during nondirected motility, independent of receptor signaling (9,10). Both forms of motility share the subcellular processes of protrusion, retraction, and cell polarization, which occur as the result of spatial and temporal coordination of molecular processes. Finally, at the cellular level, the displacements of all eukaryotic cells during nondirected motility are not truly random but instead contain periods of directional persistence in which the cell moves more or less in a straight line. Therefore, the movements of the cells during nondirected motility are often described as a persistent random walk (2). Conversely, the movements of cells undergoing chemotaxis are not perfectly directed but contain random reorientations and therefore are best described as a biased random walk (1,7). Both forms of motility, therefore, contain directional persistence and elements of randomness that give rise to reorientations.

Submitted December 17, 2009, and accepted for publication March 11, 2010.

△J. Scott Gruver and Alka A. Potdar contributed equally to this work.

*Correspondence: chang.chung@vanderbilt.edu

Editor: Alexander Mogilner.

0006-3495/10/07/0367/10 $2.00

doi: 10.1016/j.bpj.2010.03.073

Because of these commonalities, it is desirable to identify an analytical framework applicable to both forms of motility and therefore potentially capable of revealing unifying principles that govern the full range of eukaryotic cell motility. The persistence and randomness present in both forms of motility prompted us to apply bimodal analysis (11), which segregates the movements of a cell into alternating directional and reorientation modes based on the direction in which the cell is traveling. Bimodal analysis offers several advantages over existing methods of analyzing cell motility, most particularly that being the estimation of persistence time from the persistent random walk (PRW) model.

First, bimodal analysis is based on the simple assumption that cells move for some time with directional persistence and with the lack of persistence. Although an applicable theoretical model of motility is highly desirable, a recent study has cast doubt on the general applicability of the original PRW model, and even suggests that one may be required to derive a model specific to the properties of each individual cell line (3). Such a conclusion makes a model-free method, such as bimodal analysis, attractive.

Second, by treating directional and reorientation modes independently, bimodal analysis offers a measurement not only of some characteristic time for persistent motility but also for reorientation.

We exploited these advantages to compare the average time spent in directional mode to the average time spent in reorientation mode for wild-type *Dictyostelium* cells during both nondirected and chemotactic motility. Despite the fact that the mean reorientation mode time is free to vary independently of mean directional mode time, we found them to be locked into a nonlinear negative correlation. On a log-log scale, the relationship between the mean mode times appears linear, revealing that all forms of motility are described by a simple scaling law. To generalize our findings, we show the same scaling law to describe the nondirected motility of three human cell lines. We propose this scaling law to be the signature of a mechanism that gives rise to the full range of nondirected and chemotactic cell motility.

METHODS

Cell motility assays and cell tracking

The imaging of *Dictyostelium* cells and the particulars of the micropipette and microfluidic assays was previously described in Gruver et al. (12). All assays in a microfluidic device used the same flow rate as in Gruver et al. (12). Using a Rayleigh test, there was no evidence that the presence of flow directionally biased the movements of cells (data not shown). For *wt* cells and mutants, developed nondirected and micropipette assays were performed after 5 h pulsing with cAMP. The exceptions to this were $g\alpha2^-$ and aca^- mutants, which were allowed to develop for longer periods. Upon the onset of streaming and aggregation, time-lapse imaging initiated and cells were tracked as they approached the aggregation center. All time-lapse images were obtained every 3 s using 20× differential interference contrast optics and MetaMorph (Molecular Devices, Sunnyvale, CA). Given the size of the data set, we elected to use an automated tracking routine (the Track Objects function in MetaMorph) to track *Dictyostelium* cells. Care was taken to adjust the tracking parameters to reduce obvious errors in centroid estimation. *Dictyostelium* cells were tracked for a minimum of 10 min but were often tracked for up to 1 h. Blebbistatin was used to inhibit myosin II function at a concentration of 16 μM and nocodazole was used to disrupt microtubules at a concentration of 15 μM. For neutrophils (HL60), substrates were pretreated with 100 μg/mL FN for 1 h. MCF10A cells were imaged every 0.5 min and were tracked manually as previously described in Potdar et al. (11).

Fibrosarcoma cells (HT1080) were plated on culture dishes coated with 2.5 μg/mL FN. HT1080 cells were imaged every 2 min over a 4–6 h experiment with 10× objective. HT1080 cell centroids were manually tracked using the "Measure XYZ distance" function in MetaMorph. The size of the data set and the experimental parameters varied between each cell line and we chose our tracking methods pragmatically. We elected to use automated tracking in the analysis of *Dictyostelium* and neutrophils where relatively high frame rates appeared necessary to capture details. Cells were imaged using differential interference contrast optics, which allows for subpixel determination of the cell centroid and automated tracking in MetaMorph. Although the exact nature of the tracking error is unknown, we expect the relative error in the displacements obtained by automated tracking to be inversely proportional to the magnitude of displacement. MCF10A and HT1080 cells were imaged using phase contrast which prevented the use of automated tracking. Therefore, these slower moving cells were tracked manually with pixel resolution. Care was taken to increase the sampling interval so that the typical movement was considerably larger than the resolution. This, in conjunction with the larger size of these cells, increased the accuracy of manual tracking.

Bimodal analysis

Bimodal analysis, which segregates a cell path into alternating directional and reorientation modes, is fully described in Potdar et al. (11). Briefly, the first step in isolating directional and reorientation modes requires the determination of the instantaneous direction change, φ, for every time point, t. The values of $\varphi(t)$ are then compared to an empirically defined cutoff angle, φ_{cut}, with time points with values of $\varphi(t) < \varphi_{cut}$ becoming candidates for a directional mode. A second criteria is then applied, requiring at least three successive time points with $\varphi(t) < \varphi_{cut}$ before defining a directional mode. All other movements belong to reorientation modes. A range of values for φ_{cut} were tested (see Fig. S3 in the Supporting Material). In this article, the value for φ_{cut} was set to 45°. In all four cell lines used in this study, all parameters used in bimodal analysis were determined to be optimal at consistently isolated apparent modes according to visual inspection. The reorientation angle, θ, is computed as the angle between two successive directional modes (Fig. S5). The overall direction of a directional mode was determined using a multipoint linear regression of all the data points in that particular mode. Software performing bimodal analysis is available upon request.

Statistical analysis

All statistical analyses were done in MATLAB (The MathWorks, Natick, MA). Correlation coefficients, r, and their associated p values were computed using the function corrcoef.m. Slopes (scaling exponents β) were estimated and compared by analysis of covariance (ANCOVA; function aoctool.m). If significant differences within the entire dataset were detected by ANCOVA (i.e., the p value of interaction term <0.05), pairwise multiple comparisons were then made by a t statistic. This statistic was defined as the ratio of the difference of the slopes estimates to the pooled standard error for each estimate (i.e., corrected for different sample sizes for each genotype/cell line). With the exception of $pi3k1/2^-$, the residuals from all fits were shown to be normally distributed by the Lilliefors test (lillietest.m). Comparisons of the probability distributions of and for different assays were

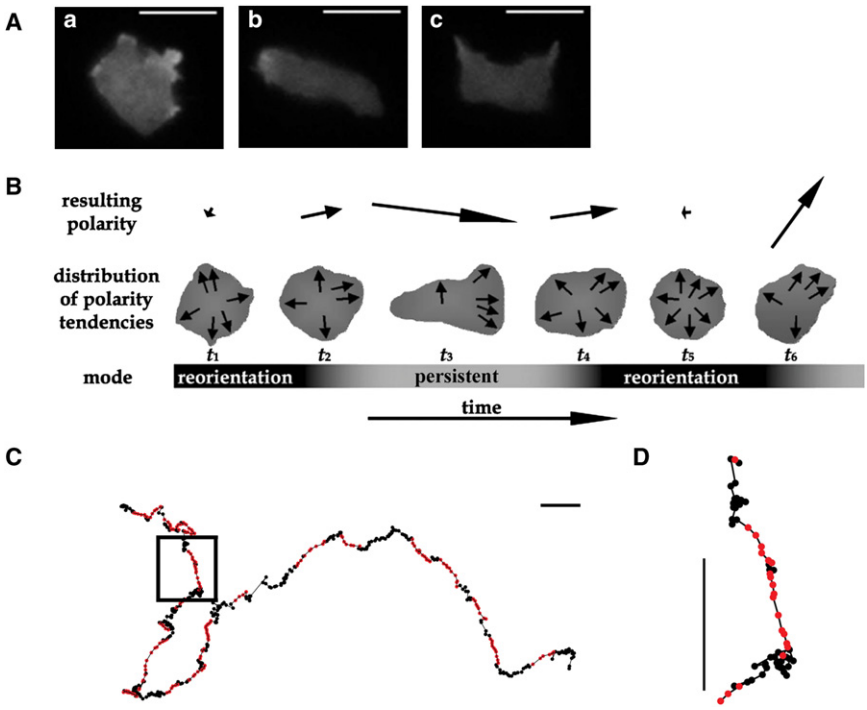

FIGURE 1 The application of bimodal analysis to directed and nondirected eukaryotic cell motility. (*A*) Images of a single *wt* cell expressing mRFP-LimE-Δ-coil. (*a*) A cell with actin polymerization randomly distributed around its cortex. (*b*) A later image of the same cell with organized leading edge and coordinated motility. (*c*) Eventually, the subcellular organization is lost. (*B*) A conceptual model for bimodal motility. During reorientation mode, a cell produces a number of competing tendencies to move in various directions, resulting in uncoordinated motion with little directional persistence. The exit from reorientation mode requires a spontaneous eruption of polarity, resulting in increased directional persistence. The polarity, however, is unstable and eventually the cell returns to reorientation mode. (*C*) An example of bimodal analysis applied to a *wt Dictyostelium* cell during nondirected migration with a three-second sampling interval over 26 min. Black points represent reorientation modes while red points represent directional modes. (*D*) The boxed region of panel *C*, showing in detail the classification into directional and reorientations modes. All scale bars are 10 μm.

compared using a Kolmogorov-Smirnoff test for two identical distributions (kstest2.m). The dispersion of the turn-angle distributions were compared using a custom randomization test (available upon request).

Simulation of persistent random walk

Cell migration is most commonly and widely described as a persistent random walk motion (3), which is emergent from the Langevin equation for a passive particle (13,14),

$$m\frac{d\vec{v}(t)}{dt} = -\xi\vec{v}(t) + \vec{f}(t), \qquad (1)$$

where m is the particle mass, $\vec{v}(t)$ is the velocity, ξ is an effective friction coefficient, and $\vec{f}(t)$ is random force acting on the particle. The first term on the right-hand side denotes the friction force that the particle experiences due to the motion in a given medium. The second term denotes the random stochastic force, which has two characteristic properties: 1), a mean of zero $\langle\vec{f}(t)\rangle = 0$; and 2), δ-functional correlations (14),

$$\langle\vec{f}(t) \times \vec{f}(t')\rangle = 2n\xi\ k_{\mathrm{B}}T\,\delta(t-t'),$$

where k_{B} is the Boltzmann constant, T is the absolute temperature, and n is the dimensionality. Although the model was developed to describe the motion of passive particles, it has long served as the starting point for the development of mathematical models for the motion of cells, which are the result of active processes (15).

Uhlenbeck and Ornstein (16) showed that mean-squared displacement,

$$\langle\Delta\mathbf{r}(t)^2\rangle,$$

can be obtained by integrating the simplified stochastic differential equation (Eq. 1) to yield

$$\langle\Delta\mathbf{r}(t)^2\rangle = \frac{2m\ k_{\mathrm{B}}T}{\xi^2}\left(\frac{\xi}{m}t - 1 + \exp(-\xi t/m)\right). \qquad (2)$$

Using the equipartition theorem,

$$k_{\mathrm{B}}T = m\langle v^2\rangle,$$

and redefining m/ξ as P, we obtain the equation

$$\langle\Delta\mathbf{r}(t)^2\rangle = 2\langle v^2\rangle P(t - P + P\exp(-t/P)), \qquad (3)$$

where P is the persistence time.

In Fig. S1, we numerically solved Eq. 1 to perform a PRW simulation of a range of persistent times and speed.

RESULTS

In an effort to understand the subcellular processes that give rise to directional persistence during both nondirected and chemotactic motility in *Dictyostelium*, we examined the dynamic localization of mRFP-labeled F-actin-binding domain of LimE (17) in wild-type (*wt*) cells. Interestingly, during nondirected motility, oscillations between two distinct patterns of localization were clearly seen within a single cell (Fig. 1 *A* and Movie S1). For periods of time, a cell would polymerize actin in brief pulses leading to protrusions at random locations around its cortex, leading to multiple competing protrusions and little net translocation of the cell (Fig. 1 *A a*). Occasionally, polymerization would occur within one region of the cell, allowing for the accumulation of polarity and persistent motility (Fig. 1 *A b*). A similar relationship between the dynamics of spontaneous PI3K signaling and directional persistence has been seen in fibroblasts during nondirected motility (18). Over time, the polarity and the persistent motility dissipated and the cell returned to its more disorganized state (Fig. 1 *A c*). Similar

oscillations between organized and disordered actin polymerization were seen during chemotaxis, although they were less pronounced (data not shown). These observations led to a conceptual model of motility as repeated symmetry breaking, i.e., a repeated transition between a reorientation mode with spatially disorganized protrusions (high symmetry) and directional mode associated with higher cell polarity and efficient motility (low symmetry).

The presence of two motility modes prompted us to apply bimodal analysis (11) to classify the displacements of individual *wt Dictyostelium* cells as belonging to either a directionally persistent or a reorientation mode. *Dictyostelium* cells move rapidly because of constant remodeling of the actin-rich cortex and concomitant changes in morphology. An example of the analysis on nondirected motility of a *wt* cell is shown in Fig. 1, *C* and *D*. The analysis identifies directionally persistent movements which are associated with the spontaneous cell polarization. Also identified are reorientation modes, which consist of movements in which the cell has temporarily lost a degree of polarity and therefore lost directional persistence. It should be noted that, in addition to consisting of movements that reorient the cell, our reorientation modes consist of movements that do not necessarily dramatically reorient the cell but, according to our model, possess the capacity to do so. To look for general principles potentially underlying the wide range of motility available to *Dictyostelium*, we analyzed data from both nondirected and chemotactic motility (see Table S1 for assays and sample sizes).

In contrast to the estimation of overall persistence time (4), bimodal analysis treats directional and reorientation modes as separate processes, and therefore provides independent measurements of the mean time spent in both directional mode, $\langle t_d \rangle$, and in reorientation mode, $\langle t_r \rangle$. The brackets indicate taking the average over the entire trajectory for a single cell. Despite the fact that $\langle t_d \rangle$ and $\langle t_r \rangle$ are free to vary independently, as evidenced by a PRW simulation (Fig. S1), we found a strong inverse relationship between them (Fig. 2 *A*). The relationship between $\langle t_d \rangle$ and $\langle t_r \rangle$ has an immediate biological consequence: it suggests the subcellular processes that govern the eruption and the dissipation of directional mode are coupled, inasmuch as an increase in $\langle t_d \rangle$ requires a reduction in $\langle t_r \rangle$. We attempted to fit the data to several common models. For example, an exponential model fit poorly (see Fig. S2). A log-log plot transforms the data, revealing a scaling relationship (i.e., $\langle t_r \rangle = C\langle t_d \rangle^{\beta}$) such as is commonly seen in complex systems near critical points (19). The inverse scaling relationship seen here for cells directly contrasts with the positive scaling relationship between search and motion phases (akin to our reorientation and directional modes, respectively) in animal foraging (20). Neither the estimate of β, nor the quality of the model fit, were drastically dependent on the value of the cutoff angle, φ_{cut} (Fig. S3). Remarkably, this representation allows for an elegantly simple description of the data from both nondirected motility and chemotaxis by a single scaling exponent (i.e., the slope of the line) of $\beta = -1.11$ (Fig. 2 *A*, *inset*, and Fig. 2 *B*).

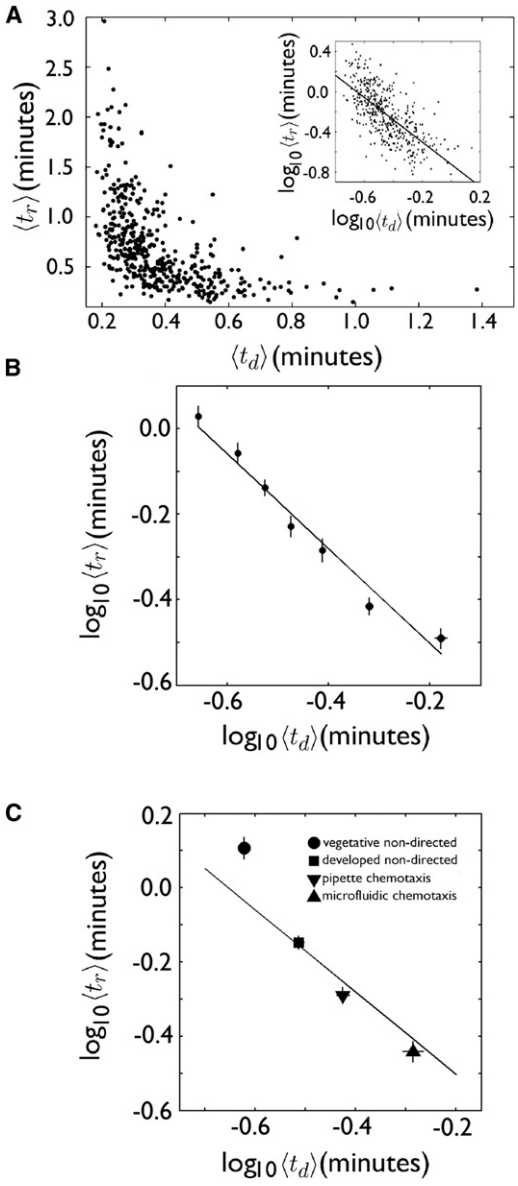

FIGURE 2 A scaling law between mean mode times. (*A*) A nonlinear relationship exists between mean directional time, $\langle t_d \rangle$, versus mean reorientation time, $\langle t_r \rangle$, from 446 *wt Dictyostelium* cells from six different motility assays. (*Inset*) A log-log plot transforms the data and allows for the estimation of the scaling exponent $\beta = -1.11$. (*B*) A plot of the data binned on the *x* axis into seven equal-sized bins. The mean ± SE of each bin is shown. The line is from the fit to the scatter plot as shown in panel *A*. (*C*) The scaling law describes the full range of *Dictyostelium* motility, including directed and nondirected motility. The means ± SE for each assay are shown.

The curve shown in Fig. 2 *A* provides a unifying description of the full range of directional persistence of *Dictyostelium* cells, including both chemotaxis and nondirected motility. In Fig. 2 *C*, the mean mode times for nondirected-vegetative, nondirected-developed, and chemotaxing

wt cells in a micropipette assay and in a microfluidic device are shown. Developed *Dictyostelium* cells are known, on average, to move faster and with greater coordination than vegetative cells (21). Likewise, developed cells are known to move faster when undergoing chemotaxis as compared to nondirected motility. Additionally, we recently showed that *wt* cells performed chemotaxis with greater efficiency in the microfluidic device compared to the micropipette assay (12). Consistent with these expectations, as the coordination of the motility is increased from vegetative nondirected motility to chemotaxis, the position of the cells on the curve slides to the right, indicating increased directional time and decreased reorientation time. The mean mode time for cells undergoing chemokinesis were essentially the same as developed cells undergoing nondirected motility (not shown).

Because all aspects of nondirected motility arise from intrinsic cell processes, the observation of a scaling relationship during nondirected motility reveals the mechanism relating $\langle t_d \rangle$ to $\langle t_r \rangle$ to be an intrinsic property of the cell. When considered separately, the presence of the same scaling law in each assay (Fig. S4 and Table S3), even in nondirected motility, indicates that cell-to-cell variability is also described by this law. Exactly what intrinsic processes are varied from cell-to-cell or from vegetative to developed cells during nondirected motility is not clear. However, the fact that cells undergoing chemotaxis also fall on this scaling curve (Fig. 2 *B*) suggests that chemoattractant-driven signal transduction harnesses these intrinsic processes (and its cell-to-cell variability) while tuning their specific properties, to increase directional persistence and reduce reorientations.

If a particular molecular pathway is responsible for coupling $\langle t_d \rangle$ to $\langle t_r \rangle$, genetic or pharmacological perturbation of that pathway might be expected to eliminate directional persistence, and therefore $\langle t_d \rangle$, during nondirected motility. Additionally, a perturbation might sever or differentially tune the coupling of $\langle t_d \rangle$ and $\langle t_r \rangle$, and thereby eliminate or alter the scaling relationship. To address the effect of perturbations on the mechanism relating $\langle t_d \rangle$ to $\langle t_r \rangle$, we examined the relationship between $\langle t_d \rangle$ and $\langle t_r \rangle$ for a total of 17 genetic mutants or cells treated with pharmacological inhibitors in vegetative-nondirected and developed-nondirected motility in pipette-chemotaxis assays. We chose cells lacking signal transduction molecules reported to be important for chemotaxis and established cytoskeletal regulators (see Fig. 3 *A* and Table S1 for a list and sample sizes). We were unable to find a mutant whose directional persistence was eliminated, suggesting the cycling between directional and reorientation modes to be a robust property of the cell. Perhaps more surprisingly, all perturbations retained a significant scaling relationship between $\langle t_d \rangle$ and $\langle t_r \rangle$ (see Fig. 3 *A* and Table S3). However, four perturbations, i.e., loss of GSK3, PTEN, or WASP, and inhibition of myosin II by blebbistatin, resulted in statistically different values for β (Fig. 3 *A*). We note that

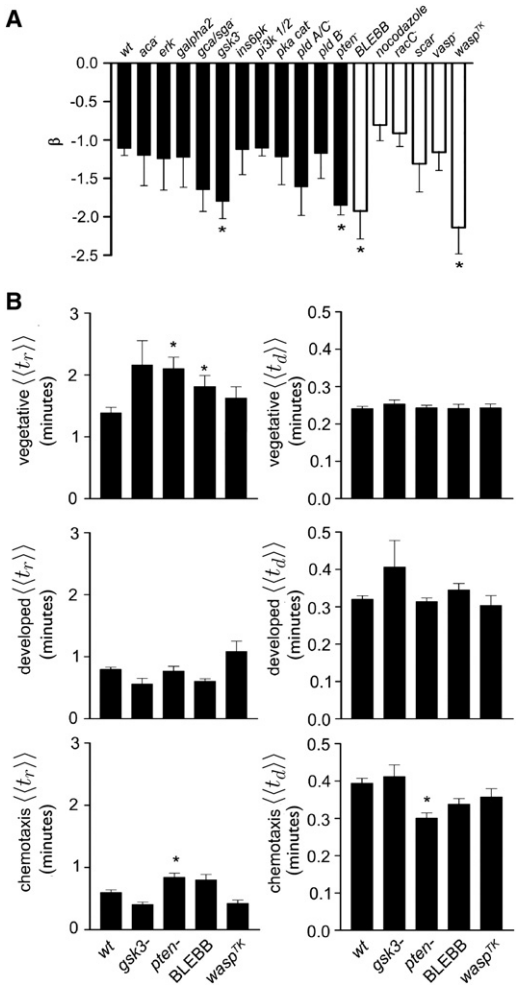

FIGURE 3 Analysis of scaling in mutants. (*A*) The values of the scaling exponent β plus the standard error of the estimates for all perturbations. Perturbations are grouped by signal transduction (*solid bars*) and cytoskeletal regulators (*open bars*). See Table S3 for details. (*B*) Comparison of $\langle\langle t_d \rangle\rangle$ and $\langle\langle t_r \rangle\rangle$ for the four mutants in vegetative nondirected (*top*), developed nondirected (*middle*), and developed chemotaxis (*bottom*). For both panels *A* and *B*, the star indicates statistical difference from *wt* at the $p < 0.05$ level.

each of these perturbations has been reported to reduce the cytoskeletal and morphological polarity thought to be critical for efficient, coordinated motility (22–25).

The scaling exponent β describes the behavior of the cells in three separate motility assays, i.e., vegetative-nondirected, developed-nondirected, and developed-chemotaxis. The steeper slope seen in the four perturbations with significantly altered scaling could come from an increase in $\langle t_r \rangle$, decrease in $\langle t_d \rangle$, or both. We examined the behavior of the four mutants that are different from *wt* in more detail in an attempt to isolate the defect to a single motility assay (e.g., vegetative nondirected motility). To do this, we compared the mean mode time, $\langle\langle t_{\mathrm{mode}} \rangle\rangle$ for each perturbation in each assay, to *wt* (Fig. 3 *B*). The double brackets indicate first averaging over the trajectory for a single cell and then averaging over

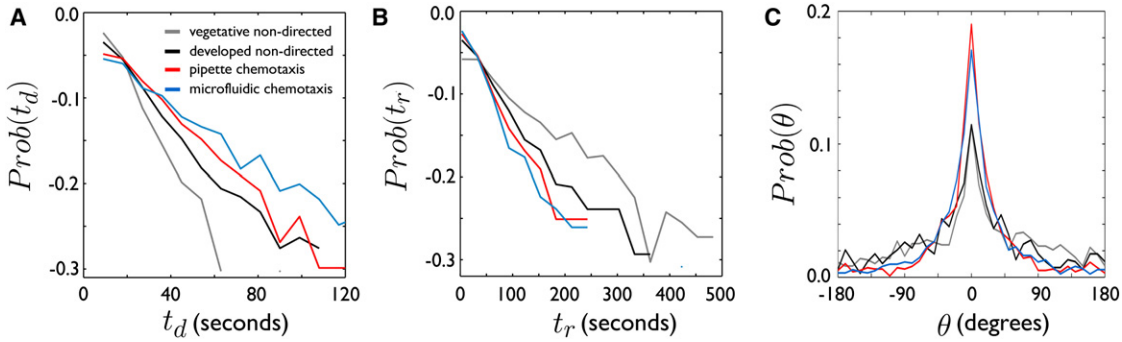

FIGURE 4 The probability distributions of directional time and reorientation angles reveals similarities and differences between directed and nondirected motility. The probability distribution of the duration of directional modes (*A*) or reorientation modes (*B*) for the vegetative nondirected, developed nondirected, developed pipette chemotaxis, and developed chemotaxis in a microfluidic device of *wt Dictyostelium* cells. (*C*) Reorientation-angle, θ, distributions for the assays in panel *A* reveal increased directional correlation between successive directional modes during directed motility.

every cell in a given assay. The *pten*$^-$ cells had a higher $\langle\langle t_r \rangle\rangle$ during vegetative nondirected motility, while, during chemotaxis, both a lower $\langle\langle t_d \rangle\rangle$ and higher $\langle\langle t_r \rangle\rangle$ contributed to a steeper scaling relationship compared to *wt*. However, removal of either data from *pten*$^-$ vegetative-nondirected motility or chemotaxis failed to return the scaling exponent of *pten*$^-$ cells to the value of *wt* (not shown). This indicates that steeper scaling relationship cannot be attributed to a single developmental stage. BLEBB-treated cells during vegetative nondirected motility had a higher $\langle\langle t_r \rangle\rangle$and lower $\langle\langle t_d \rangle\rangle$ compared to *wt*, suggesting that myosin II might be required for higher persistence in vegetative cells. Furthermore, the removal of vegetative BLEBB-treated cells from the statistical comparison of scaling exponents brought the scaling exponent of BLEBB-treated cells up to the level of *wt*. When compared in this fashion, $\langle\langle t_r \rangle\rangle$ and $\langle\langle t_d \rangle\rangle$ for both *gsk3*$^-$ and *wasp*^{TK} cells were not significantly different from *wt* in any single assay. Thus, additional highly-detailed experiments will be required to identify the source of the difference in the coupling of $\langle\langle t_r \rangle\rangle$ and $\langle\langle t_d \rangle\rangle$ in these perturbations.

The fact that both nondirected and chemotactic motility can be described by the same quantitative law suggests that chemotactic gradients serve to quantitatively tune the inherent cycling between the directional and reorientation mode. It is important to examine the nature of the cell's ability to switch between these two modes to understand the molecular mechanisms that give rise to these two modes. The probability that a cell in vegetative or developed nondirected motility and chemotaxis in the micropipette and microfluidic device will have a directional or reorientation mode of a given duration is shown in Fig. 4, *A* and *B*. The probability distributions for all four assays in Fig. 4 are qualitatively identical. In fact, the only difference revealed in Fig.4, *A* and *B*, is quantitative—i.e., an increase in typical directional mode time and a decrease in reorientation time as the cells go from vegetative to developed to chemotaxis. This strongly argues that the mechanism governing the switching between directional and reorientation modes is the same for both nondirected motility and chemotaxis. The distributions appear to be exponential, suggesting that the switching between modes occurs via a Poisson process. However, statistical support for this hypothesis was weak (not shown) indicating that perhaps a more complex mechanism is at work. This conclusion supports the conjecture that the core mechanisms governing the switching between modes are present in their most rudimentary form in vegetative cells, and that development or chemotaxis quantitatively tune these mechanisms to increase directional persistence.

The most striking difference between nondirected and chemotactic motility is revealed by considering the reorientation angle distribution, or the distribution of the angles, θ, between successive directional modes (Fig. S5) of *wt Dictyostelium* (illustrated in Fig. 4 *B*). As expected, the reorientation angle distributions for both nondirected motility and chemotaxis were symmetrical (data not shown). During vegetative and developed nondirected motility, the turn-angle distributions were peaked at ~0°, indicating that even during nondirected motility, eukaryotic cell motility has a degree of directional correlation lasting through successive directional modes. The distributions for reorientation angle also appear to be exponentially distributed, indicating that reorientation angle might follow a Poisson process. However, here too we found little statistical support for this suggestion (not shown). According to our model (Fig. 1 *B*), the transition from reorientation mode to directional mode requires the development of a comparatively ordered, subcellular polarization from a disordered state. One expectation of the bimodal model (Fig. 1 *B*) is that the magnitude of the reorientation angle would depend on the length of time the cell spent in reorientation mode, with longer reorientation modes having wider reorientation angles. Accordingly, we found that the wide turn angles were indeed associated with longer reorientations, especially for nondirected motility (Fig. S6). The reorientation angle distribution for chemotactic *wt* cells, in contrast, is less broadly dispersed despite having similar mean values. Chemotactic gradients, therefore, result in the cell spending more time in directional

mode (Fig. 4 *A*), less time in reorientation mode (Fig. 4 *B*), and an increased correlation in the direction of travel between successive directional modes.

Given the apparent generality of the mechanism relating and in *Dictyostelium*, we applied bimodal analysis to three motile human cell lines undergoing nondirected motility—i.e., neutrophils ($n = 39$), mammary epithelial cells ($n = 42$) expressing two mutant forms of the Her2 oncogene (11), and fibrosarcoma cells ($n = 19$). It should be noted that each cell was imaged with different sampling frequencies as described in Methods. Not surprisingly, these cell lines possessed different mean mode times (Fig. 5 *A*), presumably reflecting the diversity of the timescales inherent in the molecular and subcellular processes underlying motility for each cell line. All three cell lines produced significant scaling relationships with exponents similar to *Dictyostelium* (Fig. 5 *B* and Table S4). Statistical comparison of the scaling exponents revealed no significant differences between the human cell lines and *Dictyostelium*, which allowed for the estimation of a common scaling exponent for all cell lines of $\beta = -0.94$. The presence of an identical scaling exponent in these diverse cell lines indicates the work of a very general mechanism, operating across phyla and at different spatial and temporal scales, related to that in eukaryotic cells.

The possession of long directional time was proposed to increase the search efficiency of *Dictyostelium* nondirected motility (2), while efficient chemotaxis, by nature, also requires long persistence times. The ratio of $\langle t_d \rangle$ to $\langle t_r \rangle$, revealing the excess of time spent in directional mode, then, might serve as for a measure of motility efficiency. Indeed, the ratio of $\langle t_d \rangle / \langle t_r \rangle$ is a strong statistical predictor of mean cell speed over its entire trajectory for fast-moving *Dictyostelium* (correlation coefficient $r = 0.85$, significance level $p = 1.28 \times 10^{-122}$) and neutrophils ($r = 0.64$, $p = 1.30 \times 10^{-5}$), further supporting this suggestion (Fig. 5 *C* and Fig. S7). Here, for a cell with N displacements, the mean speed is defined as

$$\langle s \rangle = \frac{f}{N} \sum_{i=1}^{N} |\mathbf{d}_i|,$$

where f is the sampling frequency, and $\boldsymbol{d_i}$ is the i^{th} displacement vector. However, the ratio failed to be a significant predictor of mean speed for both mammary epithelial cells ($r = -0.20$, $p = 0.21$) and fibrosarcoma cells ($r = 0.4322$, $p = 0.065$), suggesting that speed in these slower moving cells is regulated in a different manner from the faster-moving *Dictyostelium* and neutrophils.

Mean speed in either directional mode or reorientation mode for each individual trajectory, $\langle s_{\text{mode}} \rangle$, where "mode" equal directional or reorientation, also correlated strongly with mean cell speed, $\langle s \rangle$ for all cells. The mean directional mode speed for a cell was obtained simply by estimating the mean speed of the cell during every directional mode and then taking the average over the entire trajectory.

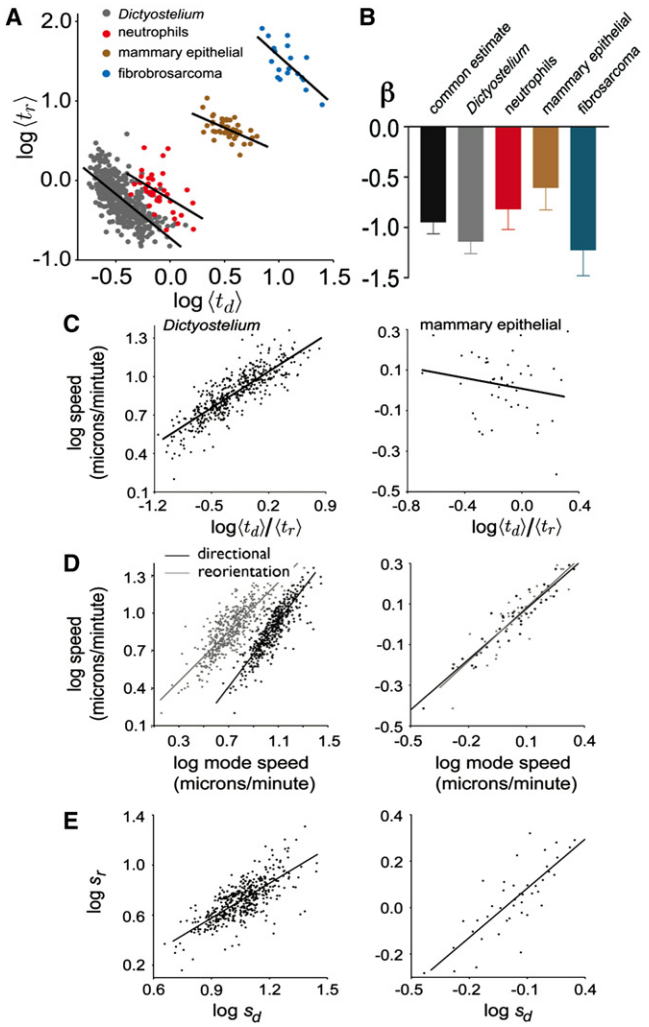

FIGURE 5 The generalization of the scaling mechanism to human cells. (*A*) Comparison of *Dictyostelium* cells, human neutrophils, mammary epithelial, and fibrosarcoma cells. (*B*) ANCOVA analysis of the scaling exponents for each cell line. The scaling exponents for each cell line were not statistically different allowing for the estimation of a common scaling exponent of $\beta = -0.938$. (*C*) The effect of bimodal motility on cell speed. The ratio of $\langle t_d \rangle / \langle t_r \rangle$ is a strong predictor of mean cell speed $\langle s \rangle$ for *Dictyostelium* (*left*) but not mammary epithelial cells (*right*). (*D*) Mean mode speeds $\langle s_{\text{mode}} \rangle$, where mode equals directional or reorientation, correlate with mean speed for both (*left*) *Dictyostelium* and mammary epithelial cells (*right*). For *Dictyostelium* cells, however, the mean speed in directional mode is significantly higher than the mean speed in reorientation mode. Thus for fast moving cells, the regulation of directional and reorientation mode effects mean speed. (*E*) A correlation between mean speed in reorientation mode and mean speed in directional mode suggests that speed is largely controlled by factors extrinsic to the regulation of bimodal motility.

The mean reorientation mode speed was defined similarly but adjusted accordingly to represent reorientation modes. Interestingly, for *Dictyostelium*, neutrophils and fibrosarcoma cells, $\langle s_d \rangle$ was found to be significantly greater than $\langle s_r \rangle$ ($p < 10^{-308}$, $p = 1.1 \times 10^{-23}$, and $p = 0.012$, respectively), indicating that higher speeds were associated with directional mode (Fig. 5 *D* and Fig. S7). This is consistent with a saltatory

model of nondirected motility in vegetative cells as suggested in Shenderov and Sheetz (26), and by our model of polarized and coordinated cytoskeletal dynamics in directional mode (Fig. 1 *B*). However, inasmuch as there was no difference between mode speeds in the mammary epithelial cells, it is evident that not all motile cells regulate their speed simply by dependence upon their motility mode.

Given that the speed of *Dictyostelium*, neutrophils, and fibrosarcoma cells is higher in directional mode than in reorientation, it is important to examine the relationship between speed in reorientation and speed directional modes. We found that there was a strong correlation between $\langle s_d \rangle$ and $\langle s_r \rangle$ for cells examined here (Fig. 5 *E*, Fig. S7, and Table S5). In fact, all the cells studied here that were relatively fast in reorientation mode were also fast in directional mode. As a result, the overall mean speed of the cell appears to be largely set by factors extrinsic to the regulation of directional and reorientation modes, despite the fact that speed can vary between modes.

DISCUSSION

With increased understanding of the detailed mechanisms regulating cell motility comes a new challenge: to integrate the findings from these diverse systems into a unified framework. Our approach provides a simple, unified description of both nondirected and chemotactic eukaryotic cell motility, and is equally applicable to other forms of directed motility. Previous attempts to unify our understanding of both directed and nondirected motility were based on the concept of receptor noise (4). However, it has since been shown that nondirected motility can take place in the absence of conventional constitutive receptor activation (9), indicating the presence of other mechanisms governing spontaneous symmetry breaking and directional persistence.

Scaling laws are often seen in complex systems near equilibrium-phase transitions and in self-organizing, nonequilibrium systems tuned near their critical points (19). The dynamics of the actin-myosin cytoskeleton have been shown to possess hallmarks of complex, nonequilibrium, self-organizing systems: scaling of mechanical behaviors (27,28); spontaneous symmetry breaking (8,29,30); and traveling waves in the form of actin polymerization and membrane protrusion (17,21,31–33). The identification of scaling behavior in a system provides significant motivation for the development of quantitative theories that start with system dynamics, attempting to explain the higher-order scaling behavior in a mechanistic fashion. The presence of a scaling law in four eukaryotic cell lines, from different phyla and tissues and each with different motility characteristics, suggests the existence of a general mechanism regulating the directional persistence (or lack thereof) in eukaryotic cell motility. The challenge now is to understand the dynamic molecular processes that give rise to directional persistence and this scaling relationship.

Our conceptual model for the formation of spontaneous polarity is similar to the model recently introduced by Weiger et al. (18). A biosensor for PI3K activity in motile fibroblasts showed that, at any given time, the cells were capable of producing multiple PI3K signaling hotspots. The dynamics of these hotspots were stochastic and the production of dominant hotspots well-correlated the directional persistence during nondirected motility. The birth and death of the hotspots were related, and they proposed a stochastic model to describe the dynamics based on a limited pool of an unknown regulator. It would be interesting to see whether a similar model, coupling stochastic dynamics to receptor-driven signaling during chemotaxis, could reproduce the relationship between nondirected and directed motility in Fig. 2.

Recent work by Bosgraaf and van Haastert (34,35) has focused on the dynamics of pseudopod extension during motility. They found that nearly all pseudopodia produced fall into one of two categories:

1. Split pseudopodia, or those that form by splitting from existing pseudopodia.
2. De novo, or those that are produced at apparently random positions around the cell cortex.

They further argue that directionally persistent motion is the result of successive split pseudopodia, whereas the interruption of directionally persistent motion is the result of de novo pseudopodia. It is an exciting possibility that our measurements of directional persistence and reorientation might be related to pseudopodia dynamics. A cursory examination of the data suggests that as cells transition from vegetative to developed, they do increase the ratio of split/de novo pseudopodia in a manner consistent with our results. In such a scenario, the scaling law would be a high-order principle that governs the ratio of split/de novo pseudopodia. However, there are a few concerns regarding any attempt to explain our scaling law strictly in terms of pseudopod production. First, the speculation about pseudopodia being the sole determinant of amoeboid motility needs to be carefully examined. Second, we succeeded in generalizing our scaling law to human epithelial and fibrosarcoma cells. It is well appreciated that such cells move slowly, with a broad and relatively stable lamella, limiting application of the idea of split/de novo pseudopodia to all motile cells. However, a more general concept of dynamical cell polarity—in which efficient, persistent motility is the result of organized, spatially restricted F-actin-based protrusion complemented with retraction—is generally applicable to all the cell lines in our study. In this scenario, the split pseudopodia are the method used by *Dictyostelium*, once the polarity has been established. Other cell lines, such as epithelial cells, utilize a more stable lamella and move at a different timescales.

The presence of persistence during vegetative nondirected motility suggests that the most basic form of spontaneous cell polarity exists in this form of motility. It seems likely

that in the vegetative state, the cellular concentrations of the key polarity components and the rate constants that govern their interaction are tuned to allow for a basic form of spontaneous polarity and directional persistence. We suggest that, in its most basic form, the ability to spontaneously polarize lies within the F-actin/myosin cytoskeleton itself and perhaps a few key regulators that initiate F-actin regulation. It is possible that these core mechanisms that give rise to spontaneous polarity are very simple given that synthetic vesicles containing F-actin have been shown to spontaneously produce pseudopodlike protrusions (36). It is here that we are likely to identify core mechanisms of spontaneous cell polarity. Our identification of four perturbations that quantitatively modify the scaling relationship provides a window into the molecular mechanism(s) that give rise to the coupling of directional and reorientation modes. The other forms of motility, i.e., those with more stable polarity and greater directional persistence, are then likely to result from the tweaking of this core system by either altering the concentrations or rate constants to further encourage spontaneous cell polarity and directional persistence or by the addition of new layers of regulation through receptor-driven or feedback-driven signal transduction.

Our results lead to the proposition that cell motility, including both directed and nondirected, results from a cycle of repeated spontaneous cell polarity. During nondirected motility, small fluctuations are amplified due to the unstable nature of the actin cytoskeleton and its core regulatory accessory molecules. These amplified fluctuations lead to cell polarity and directionally persistent motility. This cell polarity, consisting of the spontaneously orchestrated activity of numerous molecular processes distributed throughout the cell, is volatile and eventually dissipates while the underlying processes of actin regulation become uncoordinated. This lack of subcellular coordination is revealed in the lack of directional persistence during reorientation mode. During chemotaxis, concentration gradients harness this polarization-depolarization cycle to result in highly persistent, directed motility.

We propose that chemoattractant gradients, in addition to orienting the direction of polarization, either stabilize the directional mode, increase the frequency of the transition into directional mode, or both, to result in motility that appears highly directed and persistent. In this scenario, fluctuations in key F-actin regulators, such as WASP, SCAR, or Formins initiate F-actin polymerization. Single knockouts of all three of these actin polymerization initiators show defects in chemotaxis and nondirected motility. In our study, we showed that loss of WASP function, but not SCAR function, leads to a quantitatively altered scaling relationship between persistence time and reorientation time.

Dictyostelium cells are capable of detecting extremely weak gradients of chemoattractant. It has been shown that they can sense gradients in the nM range (6) with an estimated difference in receptor occupancy from anterior to posterior in the range of 130 receptors (5). Based on the assumption that the directional persistence in chemotaxis results from instructions to the cytoskeleton from signal transduction, analyses of the sensory processes concluded that chemotaxis occurs near the limit set by noise (5,7). However, feedback between the actin cytoskeleton and the gradient sensory system has been demonstrated in both *Dictyostelium* and neutrophils (9,37–40). Moreover, the treatment of *Dictyostelium* with Latrunculin, which reduces F-actin and eliminates morphological polarity, also eliminates the spontaneous activation of Ras and production of the second messenger PIP3 in the absence of chemoattractant receptor signaling (9). Thus it appears that the signal transduction system, rather than controlling, works in conjunction with cytoskeletal dynamics to produce efficient cell motility.

SUPPORTING MATERIAL

Seven figures, five tables, and one movie are available at http://www.biophysj.org/biophysj/supplemental/S0006-3495(10)00710-1.

The authors thank Dr. Leena Choi for valuable discussion and suggestions for statistical analysis.

This work was supported by grants from the National Institutes of Health (No. GM68097 to C.Y.C., and No. CA113007 to V.Q.).

REFERENCES

1. Arrieumerlou, C., and T. Meyer. 2005. A local coupling model and compass parameter for eukaryotic chemotaxis. *Dev. Cell.* 8:215–227.
2. Li, L., S. F. Nørrelykke, and E. C. Cox. 2008. Persistent cell motion in the absence of external signals: a search strategy for eukaryotic cells. *PLoS ONE.* 3:e2093.
3. Selmeczi, D., S. Mosler, …, H. Flyvbjerg. 2005. Cell motility as persistent random motion: theories from experiments. *Biophys. J.* 89:912–931.
4. Tranquillo, R. T., D. A. Lauffenburger, and S. H. Zigmond. 1988. A stochastic model for leukocyte random motility and chemotaxis based on receptor binding fluctuations. *J. Cell Biol.* 106:303–309.
5. Ueda, M., and T. Shibata. 2007. Stochastic signal processing and transduction in chemotactic response of eukaryotic cells. *Biophys. J.* 93:11–20.
6. Song, L., S. M. Nadkarni, …, E. Bodenschatz. 2006. *Dictyostelium discoideum* chemotaxis: threshold for directed motion. *Eur. J. Cell Biol.* 85:981–989.
7. van Haastert, P. J., and M. Postma. 2007. Biased random walk by stochastic fluctuations of chemoattractant-receptor interactions at the lower limit of detection. *Biophys. J.* 93:1787–1796.
8. Yam, P. T., C. A. Wilson, …, J. A. Theriot. 2007. Actin-myosin network reorganization breaks symmetry at the cell rear to spontaneously initiate polarized cell motility. *J. Cell Biol.* 178:1207–1221.
9. Sasaki, A. T., C. Janetopoulos, …, R. A. Firtel. 2007. G protein-independent Ras/PI3K/F-actin circuit regulates basic cell motility. *J. Cell Biol.* 178:185–191.
10. Weiger, M. C., C. C. Wang, …, J. M. Haugh. 2009. Spontaneous phosphoinositide 3-kinase signaling dynamics drive spreading and random migration of fibroblasts. *J. Cell Sci.* 122:313–323.
11. Potdar, A. A., J. Lu, …, P. T. Cummings. 2009. Bimodal analysis of mammary epithelial cell migration in two dimensions. *Ann. Biomed. Eng.* 37:230–245.

12. Gruver, J. S., J. P. Wikswo, and C. Y. Chung. 2008. 3′-Phosphoinositides regulate the coordination of speed and accuracy during chemotaxis. *Biophys. J.* 95:4057–4067.
13. Saltzman, W. M. 2004. Tissue Engineering: Engineering Principles for the Design of Replacement Organs and Tissues. Oxford University Press, New York.
14. Doi, M., and S. F. Edwards. 1986. The Theory of Polymer Dynamics. Oxford University Press, New York.
15. Selmeczi, D., L. Li, …, H. Flyvbjerg. 2008. Cell motility as random motion: a review. *Eur. Phys. J. Spec. Top.* 157:1–15.
16. Uhlenbeck, G. E., and L. S. Ornstein. 1930. On the theory of the Brownian motion. *Phys. Rev.* 36:823–841.
17. Bretschneider, T., S. Diez, …, G. Gerisch. 2004. Dynamic actin patterns and Arp2/3 assembly at the substrate-attached surface of motile cells. *Curr. Biol.* 14:1–10.
18. Weiger, M. C., S. Ahmed, …, J. M. Haugh. 2010. Directional persistence of cell migration coincides with stability of asymmetric intracellular signaling. *Biophys. J.* 98:67–75.
19. Bak, P., C. Tang, and K. Wiesenfeld. 1988. Self-organized criticality. *Phys. Rev. A.* 38:364–374.
20. Bénichou, O., M. Coppey, …, R. Voituriez. 2005. Optimal search strategies for hidden targets. *Phys. Rev. Lett.* 94:198101.
21. Maeda, Y. T., J. Inose, …, M. Sano. 2008. Ordered patterns of cell shape and orientational correlation during spontaneous cell migration. *PLoS ONE.* 3:e3734.
22. Etienne-Manneville, S., and A. Hall. 2003. Cdc42 regulates GSK-3β and adenomatous *Polyposis coli* to control cell polarity. *Nature.* 421:753–756.
23. Iijima, M., and P. Devreotes. 2002. Tumor suppressor PTEN mediates sensing of chemoattractant gradients. *Cell.* 109:599–610.
24. Stites, J., D. Wessels, …, D. R. Soll. 1998. Phosphorylation of the *Dictyostelium* myosin II heavy chain is necessary for maintaining cellular polarity and suppressing turning during chemotaxis. *Cell Motil. Cytoskeleton.* 39:31–51.
25. Myers, S. A., J. W. Han, …, C. Y. Chung. 2005. A *Dictyostelium* homologue of WASP is required for polarized F-actin assembly during chemotaxis. *Mol. Biol. Cell.* 16:2191–2206.
26. Shenderov, A. D., and M. P. Sheetz. 1997. Inversely correlated cycles in speed and turning in an amoeba: an oscillatory model of cell locomotion. *Biophys. J.* 72:2382–2389.
27. Fabry, B., G. N. Maksym, …, J. J. Fredberg. 2001. Scaling the microrheology of living cells. *Phys. Rev. Lett.* 87:148102.
28. Stamenović, D., N. Rosenblatt, …, D. E. Ingber. 2007. Rheological behavior of living cells is timescale-dependent. *Biophys. J.* 93: L39–L41.
29. Kozubowski, L., K. Saito, …, D. J. Lew. 2008. Symmetry-breaking polarization driven by a Cdc42p GEF-PAK complex. *Curr. Biol.* 18:1719–1726.
30. Ozbudak, E. M., A. Becskei, and A. van Oudenaarden. 2005. A system of counteracting feedback loops regulates Cdc42p activity during spontaneous cell polarization. *Dev. Cell.* 9:565–571.
31. Döbereiner, H. G., B. J. Dubin-Thaler, …, M. P. Sheetz. 2006. Lateral membrane waves constitute a universal dynamic pattern of motile cells. *Phys. Rev. Lett.* 97:038102.
32. Gerisch, G., T. Bretschneider, …, K. Anderson. 2004. Mobile actin clusters and traveling waves in cells recovering from actin depolymerization. *Biophys. J.* 87:3493–3503.
33. Weiner, O. D., W. A. Marganski, …, M. W. Kirschner. 2007. An actin-based wave generator organizes cell motility. *PLoS Biol.* 5:e221.
34. Bosgraaf, L., and P. J. Van Haastert. 2009. Navigation of chemotactic cells by parallel signaling to pseudopod persistence and orientation. *PLoS ONE.* 4:e6842.
35. Bosgraaf, L., and P. J. M. Van Haastert. 2009. The ordered extension of pseudopodia by amoeboid cells in the absence of external cues. *PLoS ONE.* 4:e5253.
36. Haeckl, W., M. Baermann, and E. Sackmann. 1998. Shape changes of self-assembled actin bilayer composite membranes. *Phys. Rev. Lett.* 80:1786–1789.
37. Sasaki, A. T., C. Chun, …, R. A. Firtel. 2004. Localized Ras signaling at the leading edge regulates PI3K, cell polarity, and directional cell movement. *J. Cell Biol.* 167:505–518.
38. Wang, F., P. Herzmark, …, H. R. Bourne. 2002. Lipid products of PI_3Ks maintain persistent cell polarity and directed motility in neutrophils. *Nat. Cell Biol.* 4:513–518.
39. Inoue, T., and T. Meyer. 2008. Synthetic activation of endogenous PI_3K and Rac identifies an AND-gate switch for cell polarization and migration. *PLoS ONE.* 3:e3068.
40. Janetopoulos, C., L. Ma, …, P. A. Iglesias. 2004. Chemoattractant-induced phosphatidylinositol 3,4,5-trisphosphate accumulation is spatially amplified and adapts, independent of the actin cytoskeleton. *Proc. Natl. Acad. Sci. USA.* 101:8951–8956.